ESTIMATING AIR INFILTRATION RATES THROUGH LARGE OPENINGS FOR IMPROVED BUILDING ENERGY USE IMPACTS EVALUATION

By

Yusuf Kemal Basmaci

A THESIS

Submitted to
Michigan State University
in partial fulfillment of the requirements
for the degree of

Civil Engineering – Master of Science

2025

ABSTRACT

Industrial buildings represent a substantial portion of building energy consumption throughout the U.S., with heating, ventilation and air conditioning (HVAC) making up approximately 9.3% of net electricity and 6% of natural gas consumption. One of the main drivers of operation and energy use of the HVAC system is infiltration. For industrial buildings, many have a substantial number of large openings for shipping and receiving, often with these doors remaining open for extended period of time. Opportunities to reduce infiltration through these openings exist, such as through the use of air or plastic curtains. However, the relative energy savings impact of the such retrofits is not standardized in part because the baseline level of unconditioned air flowing into the existing large openings is not well established. This study examines wind speed variations impact on air infiltration rates within a large opening in an industrial-style building through experimental testing, in an effort to establish an empirical relationship between weather station wind speed and the wind-driven air flow experienced through large openings. Wind speed measurements were collected from multiple sensors installed at the opening and compared with data from a nearby weather station. Results show that wind speeds at weather station height (~10 m) level (4.75 m/s) were significantly higher than those at the opening (0.72 m/s), with the lowest sensor within the opening recording the highest wind speeds. Results also suggest that compared to the estimated wind speeds based on the existing EnergyPlus Effective Area Infiltration model, air speeds measured at the large opening were 60.9% lower. A data-driven regression model was then developed to estimate wind speed at the opening based on weather-station height wind speed data, achieving an R^2 of 0.75, with cross-validation confirming its reliability. The resulting data-driven model can be used to better estimate the air speeds and thus infiltration experienced at large door openings, improving the overall ability of existing models to estimate energy implications of large door openings.

TABLE OF CONTENTS

INTRODUCTION

Buildings play a critical role in modern society, providing spaces for residential, commercial, and industrial activities. Worldwide people spend approximately 90% of their time in indoor environments (Mannan, Al-Ghamdi, 2021). This directly impacts buildings' energy demand and consumption. According to the International Energy Agency, buildings globally account for roughly 30% of energy consumption (IEA, 2025). In the U.S., where people also on average spend more than 90% of their time indoors (Dong et al., 2024) the building sector consumes about 40% of primary energy use (DOE, 2015), and 38% of carbon dioxide emissions (Andrews & Jain, 2023). It is projected that global energy consumption will increase through 2025 outpacing efficiency gains and driving continued emission growth (US EIA, 2023). Consequently, enhancing buildings' energy performance is essential for reducing energy demand and advancing sustainability. Globally, energy efficiency improved by an estimated 13% between 2000 and 2017 (IEA, 2019). In the world's major economies, the majority of these savings were obtained in the industrial and building sectors (IEA, 2019). Cities across the US are turning increasingly to mandatory policies that require improved energy efficiency and emissions performance across their existing building stock (ASHRAE, 2021).

Research on energy efficiency within the building sector has predominantly focused on residential and commercial buildings. Numerous studies have examined energy performance and efficiency measures in these sectors (e.g. NREL, 2025, Torres, 2021, Wilberforce, 2021, Brown, 2008, Economidou, 2020). In contrast, significantly less research has been conducted on industrial buildings and their energy performance (Goulis, 2016, Brinks, 2014).

Industrial facilities are designed and operated in accordance with local regulations and are influenced by the type of activities they support. The International Building Code (IBC) establishes classifications for buildings based on their use and occupancy to ensure appropriate design and safety measures; industrial buildings typically fall under Factory Industrial Group F. Group F occupancy includes the use of a "building or structure for assembling, disassembling, fabricating, finishing, manufacturing, packaging, repair or processing operations". However, buildings that store or handle hazardous materials in quantities exceeding the permissible limits are classified as Group H (High-Hazard Occupancy). Similarly, warehouses are classified under Group S (Storage Occupancy) (ICC, 2015). An industrial building may fall into one or more of these categories of building types. In terms of overall characteristics, typically, industrial facilities feature high

ceilings (ranges between 2.8 – 7.3 meters), large open floor areas to accommodate machinery, loading docks for receiving and shipping materials, and a relatively small office space compared to the overall floor area, often constituting less than 20% of the total space (NAIOP, 2024). The United States has approximately 350,000 to 400,000 manufacturing establishments, according to the U.S. Census Bureau and Bureau of Labor Statistics (U.S. Bureau of Labor Statistics, 2022). The number grew from 358,000 in 2020 to around 403,000 in 2024, reflecting industrial expansion U.S. Bureau of Labor Statistics, 2025). The manufacturing also sector employs nearly 13 million Americans as of 2025, highlighting its significant economic impact (National Association of Manufacturers, 2025).

Industrial buildings also have different thermal behavior than residential and commercial buildings due to their different building shapes, materials, interior temperatures, operation hours, and internal gains from processes and machines (Brinks, 2016). Apart from the energy used by manufacturing processes, industrial facilities consume considerable amounts of energy for non-process energy, including lighting, heating, cooling, ventilation, humidity control, and/or particulate control (Wang, Cao, & Meng, 2019, Goulis, 2016, Khalde et al, 2017). Among non-process energy-consuming systems, HVAC systems account for 9.3% of net electricity consumption and 6% of natural gas consumption in the U.S. (MECS, 2018). One of the driving factors defining how much HVAC systems are required to operate to maintain the targeted indoor environmental conditions is the exchange of air across the building envelope, from the building exterior to the interior, and vice versa (Persily et al., 2019).

The more air infiltration, defined as the uncontrolled inward leakage of outdoor, unconditioned and unfiltered air into buildings, that occurs, the more the HVAC systems must work. Additionally, infiltration affects indoor air quality (Kempton, 2022), and occupant comfort (C NG, et al, 2019). This infiltration primarily occurs through various openings in the building envelope varying from large openings such as doors and windows to small cracks and crevices (Kirimtat & Krejcar, 2018). In addition to a building envelope having more openings for air to travel through, infiltration is driven by pressure differentials created by wind, stack effect, and HVAC operations. For wind, when the wind blows against a building, it creates higher pressure on the side facing the wind and lower pressure on the opposite side. This pressure difference pushes air into the building through cracks and openings on the windward side and pulls air out from the leeward side (Sakiyama, 2024). For the stack effect, in winter, warm indoor air, being lighter than cold air, rises and escapes

through higher openings in a building, creating a low-pressure zone near the bottom. This pressure difference draws in colder outdoor air through lower openings, such as doors and cracks. In summer, the process can reverse if the indoor air is cooler than the outside air (Kosonen, et al, 2017). Even though a combination of both phenomena persists as the driving force, the pressure gradient on the facade of a building as a result of gusting wind is mostly the controlling infiltration driving force in low-rise buildings (Brownell, 2002). HVAC systems can also substantially alter the pressure distribution across the building envelope (Makawi, et a, 2023, Jokisalo, 2009, Persily, 2019).

The growing concerns over building energy use highlights the importance of controlling air leakage and estimating infiltration rates in all types of buildings including industrial. Prior research suggests that infiltration accounts for up to 40% of the total heat energy demand of industrial buildings (Brinks, 2014). In an analysis of the U.S. building stock's airtightness (300+ buildings tested), industrial facilities exhibited the highest air leakage rates on average, significantly higher than offices or schools (Emmerich and Persily, 2014). This aligns with findings from a case study on industrial facilities in China which showed that the air exchange rate was far above typical residential buildings (Sun & Yang, 2014). Given the substantial energy losses associated with infiltration, further research on industrial facilities is critical to developing more accurate models, optimizing energy performance, and informing future regulations.

Among the openings in the building envelope of a typical industrial building through which substantial infiltration can occur, the largest openings are typically external garage and loading dock doors (Daiz-Elsayed et al, 2022). However, estimating how much infiltration occurs through these openings, particularly for industrial buildings, is not well studied. In addition, some studies highlight potential misleading energy simulation results associated with infiltration when compared to measured data (Tanasic et al. 2010).

Various methodologies have been used to study air infiltration each with advantages and limitations (Abishedid, 2011). The most common experimental methods to evaluate air infiltration are blower door testing and tracer gas methods (ASTM, 2021a, 2021b). However, these are not typically used if there are large door openings in the building envelope and are used more for tighter building envelope constructions due to limitations, for example, of the flowrate of the fans used for blower door testing. Empirical models for air infiltration estimation rely on past experimental data, statistical correlations, and simplified physical assumptions to predict air

leakage in buildings (Porsani, 2024). Common empirical approaches include the air change methods (ASHRAE, 2021), the Effective Leakage Area (ELA) model (ASHRAE Standard 119, 2020) and the Sherman and Grimsrud model (Sherman & Grimsrud, 1980). Computational methods for air infiltration estimation rely on numerical simulations and mathematical models to predict airflow through building envelopes under various conditions (Lui, 2020, Chao, 2023).

However, despite its importance in the buildings sector, air infiltration calculations still involve substantial uncertainties (Jones, 2015). Infiltration is particularly problematic in industrial buildings, where large doors and ventilation openings create complex airflow patterns that are difficult to manage (Banti, 2024). Specialized publications about wind-driven measurements infiltration of industrial buildings are rare (Sun & Yang, 2014). Moreover, commonly used energy modeling tools, such as EnergyPlus, rely on models (Effective Leakage Area Model, DOE-2 Infiltration Model, and BLAST Infiltration Model) based on empirical equations for estimating infiltration, which were all primarily developed based on low-rise residential buildings. The relationship between wind speed observed at weather station height and infiltration through these large openings thus remains underexplored (Gowri, 2009), further contributing to the gap in accurately estimating infiltration in industrial facilities (Persily et al., 2019). Hayati (2017) also noted that two of the most advanced air infiltration models (LBL, AIM-2 model) along with their variants (LBLNPL, AIM-2Crawl), tend to overpredict infiltration rates in large buildings. There thus remains a gap in research regarding the estimation of infiltration rates through large openings in industrial buildings. Understanding the wind flow pattern across these openings is essential for improving and calibrating existing models. Improved estimates also help to better estimate the energy impact of retrofits such as plastic and air curtains in these openings. This study thus aims to study wind-driven infiltration through large openings in industrial buildings, in an effort to provide better simplified methods of estimating infiltration based on widely available weather data. By employing high-accuracy anemometers at different heights in a large opening, this research supports an assessment of the airflow profile of infiltration into an industrial-style building as compared to measured wind speed data yielding a method of estimation of infiltration given local wind data. The remainder of this research is structured as follows. Section 2 provides an overview of the methodology used. Section 3 presents data analysis and results discussion. Finally, Section 4 concludes the study by summarizing the findings and suggesting directions for future research.

METHODOLOGY

Research was conducted in a single-zone industrial building with an overhead door, where high-precision anemometers were placed at different heights, along with a rooftop sensor for comparison with local AWOS weather station data. Data was collected over a range of conditions and analyzed to compare variations in air flow through the opening across all sensors and in comparison to the weather station-height wind speed data. Regression models were then developed using experimental and weather station data to create a predictive framework for wind speed at the opening level, which is then used in infiltration models to estimate infiltration rates using weather data.

Experimental Setup

The experiment was conducted in East Lansing, Michigan. This location has a cool-humid climate (ASHRAE Climate Zone 5A). The ASHRAE design conditions for Climate Zone 5A, derived from ASHRAE Climate Data, provide key parameters for HVAC system sizing and energy modeling. For heating design, the 99.6% and 99% heating dry-bulb temperatures are -17.9°C and -15.0°C, respectively. The extreme minimum dry-bulb temperature is -22.8°C, providing a reference for winter design conditions. For cooling design, the 0.4% and 1% cooling dry-bulb temperatures are 32.0°C and 30.2°C. The average annual wind speed measured at 10 m is estimated to be 2.7 m/s (ASHRAE, 2021). By contrast Climate Zone 1A (Very Hot-Humid), which includes regions like southern Florida, experiences relatively low average wind speeds, typically around 3–4 m/s. In contrast, Climate Zone 7 (Very Cold), covering parts of North Dakota and Minnesota, sees considerably higher average wind speeds, averaging between 5–6 m/s (ASHRAE, 2021). Therefore, the wind experienced in this region represents approximately average conditions across the U.S.

The experiment location is in a suburban area dominated by low-rise buildings and large open fields, with no tall surrounding structures. The experimental building is 10.5 meters in height, 21 meters in length and 15 meters in width. The building has two large openings with overhead doors, with the larger opening with overhead door facing west, measuring 3.66 m in width and 4.30 m in height, typical of industrial facilities such as warehouses, manufacturing plants, or distribution centers (NAIOP, 2024). There is no established standard dimension for large openings or dock doors in industrial facilities. However, as they are commonly used for shipment purposes, these dock doors are typically designed to accommodate trucks backing up for loading and unloading.

According to the Department of Transportation, most truck height limits range from 4.11 meters to 4.27 meters, making the opening used in this experiment well-suited to be considered a "standard" dock door (DOT, 2004).

To ensure accurate airflow measurement, the building's ventilation and heating systems were turned off during experimental testing, meaning that the airflow patterns were not impacted by HVAC operations. For monitoring airflow through the opening, a digital manometer (RetroTech DM32) was employed to measure the pressure difference between the interior and exterior of the building on the west face of the building. The pressure difference between the indoor and outdoor environments was measured multiple times during the experiment during periods of low to no wind; during these times the differential pressure did not exceed 5 Pa.

To measure airflow through the opening, high precision anemometers (METER-ATMOS22) were used. The chosen sensors have the ability to sample data at a high frequency (0.015 seconds), include a measurement range of 0-30 m/s, a resolution of 0.01 m/s, and an accuracy of ±3% (METER, 2023). These specifications were considered to be acceptable as they meet or exceed the specifications used for the sensors used to support the U.S. Weather Observing System (AWOS) (FAA, 2017) as shown in Table 1. For experimental testing, data was recorded at a frequency of 5 seconds using a CR1000X datalogger (Campbell Scientific, 2024).

Table 1. Technical Specifications of Anemometer and AWOS System

Sensor Model	Accuracy (%)	Resolution (m/sec)	Measuring Frequency (sec)	Range (m/sec)
METER-ATMOS22 (used for experimental testing)	±3.0%	1.22	0.015	0 - 30
AWOS	±2.4%	0.50	0.400	0.5 - 44

Five sensors were deployed. Four were installed within the large opening, and one was mounted on the building's roof. The rooftop sensor was used for comparison with the nearest AWOS weather station. Capital Region International Airport (KLAN) is the closest AWOS weather stations to the experiment site, located approximately 15 km away (NWS, 2025). AWOS weather stations typically mount wind speed sensors at a height of 10 meters (FAA, 2017). To ensure a valid comparison with the KLAN weather station, the rooftop sensor was mounted on a 3-meter

tripod. Given that the building's roof is 10 meters heigh, this setup positioned the sensor at a total height of approximately 13 meters. This configuration also meets the Federal Aviation Administration criteria for AWOS stations, ensuring that all surrounding obstructions (e.g., vegetation, buildings, etc.) were at least 4.57 meters lower than the sensor height reducing localized interference (FAA, 2017). The tripod was secured using mounting brackets and heavy-duty straps, with all fasteners tightened to withstand strong weather conditions. Additionally, the tripod was anchored at the building's corner to ensure proper alignment with the sensors installed. The sensors were then numbered sequentially as S1, S2, S3, S4, and S5, corresponding to increasing height. S1 was placed at the lowest height, while S5 was positioned at the roof at the highest elevation. A wooden structure was built to securely mount the sensors at various heights for S1 through S4.

The sensors were positioned withing the large opening to ensure accurate airflow measurements while reducing the impact of airflow around the edges. Studies have shown that airflow near the boundaries of large openings exhibits turbulence and irregular wind profiles due to interactions with structural surfaces, which can affect measurement accuracy (Hayati et al., 2017). To mitigate these effects, the sensors were placed away from the edges, aiming for a more stable and representative airflow assessment. Specifically, Sensors 2 and 3 were positioned 1.22 meters away from the vertical edges, corresponding to approximately one-third of the opening width, while Sensors 1 and 4 were located at the center of the opening's width.

Previous research has demonstrated that airflow distribution varies significantly with height in large openings, necessitating a vertical distribution of sensors to capture these variations effectively (Deng & Tan, 2019, Allard & Utsumi, 1992). To account for these variations, the sensors were placed at three heights: the first at approximately one-fourth of the opening height, the second level at half the height, and the third at three-fourths of the height. Table 2 shows the positioning of the sensors. Figure 1a also provides a visual representation of how the sensors were configured and the associated dimensions. Figure 1b shows the actual experimental setup.

Table 2. Spatial Configuration of Sensors Installed on the Gate and Roof, Including Heights and Distances from Opening Edges

Sensors	Sensor ID	Sensor Height (m)	Distance from Opening Edges (m)			
			Right Edge	Left Edge	Top Edge	Bottom Edge
Sensor 1	S1	1.22	1.83	1.83	3.08	1.22
Sensor 2	S2	2.44	2.44	1.22	1.86	1.22
Sensor 3	S3	2.44	1.22	2.44	1.86	1.22
Sensor 4	S4	3.66	1.83	1.83	1.22	3.08
Sensor 5 (Roof)	S5	13.0	-	-	-	-

Data was collected in April 2024. Data was collected over seven consecutive days, from April 5, 2024, to April 11, 2024, between 11:30 am and 01:00 pm daily, resulting in 48,000 total data points collected during this period. In addition to the sensors' data collected from the building, weather data from one of the closest AWOS stations were collected (same time interval) to compare with the rooftop sensor measurements. Capital Region International Airport (KLAN), located approximately 15 km from the experiment site, was selected as the reference AWOS station for this comparison (NWS, 2025).

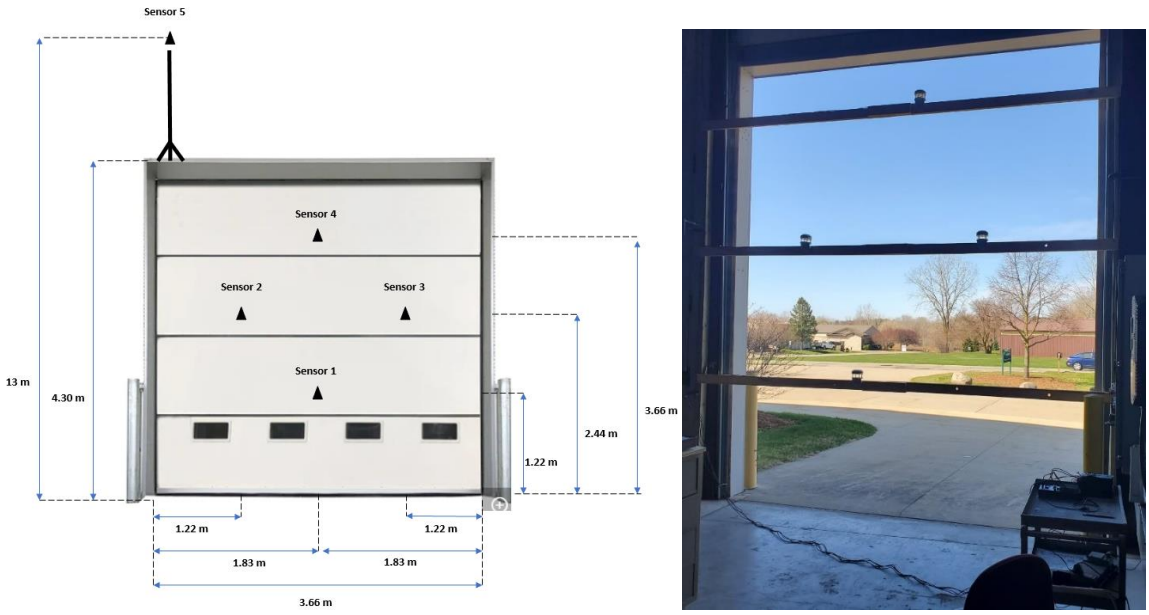

(a) (b)

Figure 1: (a) Schematic Representation of Sensor Configuration and Dimensions (b) Photograph of the Actual Experimental Setup Data Cleaning and Processing

For the analysis, Python was utilized to process and interpret data. Key libraries, including pandas (for data manipulation), matplotlib (for data visualization), and scikit-learn (for data analysis and modeling), were employed to extract insights from the collected measurements. The data in was first cleaned and processed prior to analysis across all sensors. The raw data contained 48,000 data points collected at 5 second intervals. A total of 80 invalid data points (negative or NA values) were identified and removed, representing 0.2% of the total data points. The invalid data was removed prior to further analysis.

To ensure consistency, data cleaning also included matching data points from the same time intervals across all sensors as the data collected on different days were sometimes misaligned by a few seconds. This process ensured that the analysis was based on synchronized data points, maintaining a uniform frequency of 5 second. The data was then converted to a 5-minute frequency by averaging the wind speed recorded every 5 seconds within each interval. This conversion was completed in order to be able to be compared to the closet AWOS weather station (KLAN) which is also collected a 5-minute frequency.

Once the data was cleaned and synchronized, several calculations were performed to analyze the wind speed measurements. First, the daily average wind speed was determined for each sensor individually. Additionally, the daily average wind speed for the four sensors installed on the gate (S1, S2, S3, and S4) was calculated as a combined value to represent the overall wind conditions at the opening. The daily average wind speed recorded by the AWOS weather station was also computed for comparison. Following this, the average wind speed over the entire experimental period was calculated for each sensor, the combined sensors, and the AWOS weather station. Furthermore, the median and standard deviation were determined for all these values to assess the variability and distribution of wind speed across the different measurement points.

Using these wind speed measurements, the infiltration rate (m^3/s) was then calculated using an EnergyPlus wind-drive infiltration model "Effective Leakage Area Model" (DOE, 2022) The model calculates the infiltration airflow rate (Q) using Equation 1

$$Q = \mathrm{C} \times A \times U_h \qquad \text{(Equation 1)}$$

where Q is infiltration rate (m^3/s), C is discharge coefficient (typically ranges between 0.6 and 0.7 for large openings), A is area of the opening (m^2), and U_h is wind speed perpendicular to the opening (m/s). The equation provides a simplified approach to estimating wind-driven infiltration by assuming that airflow is directly proportional to wind speed. This method streamlines the estimation process by focusing on wind speed, thereby omitting the need for complex pressure differential calculations.

Next, to evaluate how well current the current methods estimate U_h compared to the measured field data from S1 through S4, windspeed data from the closest AWOS weather station during the experimental period was obtained, and adjusted to estimate the wind speed at the experimental location height, following the procedure outlined in the DOE Engineering Reference (DOE, 2022), as shown in Equation 2

$$U_h = U_{met} \left(\frac{\delta_{met}}{z_{met}}\right)^{\alpha_{met}} \times \left(\frac{z}{\delta}\right)^{\alpha} \qquad \text{(Equation 2)}$$

Where: U_h is average local wind speed at height h (m/s), U_{met} is wind speed from meteorological weather station, Z_{met} is height of the standard meteorological weather station (assumed 10 m), z is the height of the opening/door (measured as 4.30 m), $\alpha \; and \; \alpha_{met}$ are terrain dependent coefficient

for the experiment location and the meteorological weather station (assumed 0.14 and 0.33 respectively), and δ, δ_{met} are boundary layer thickness for the given terrain type (assumed 270 m and 460 m respectively) (DOE, 2022). This conversion accounts for the difference in elevation between the meteorological measurement height (z_{met}) and the opening height (z) by applying a terrain-dependent power-law relationship. The terrain-dependent coefficients (α, α_{met}) and boundary layer thickness values (δ, , δ_{met}) are included to adjust for differences in surface roughness between the weather station location and the experimental site (DOE, 2022). The terrain for the weather station was assumed to be flat and open, while the terrain for the experiment location was assumed to be of towns and cities.

The collected data is then used to develop data-driven models for estimating wind speed at the experimental location. These models utilize statistical and regression-based techniques to establish relationships between recorded sensor data and external weather station measurements. Models are then evaluated using cross validation to determine how well the models perform using different subsets of data to create and evaluate the models. The estimated wind speed from these models is then used to calculate the infiltration rate through the opening.

RESULTS

Results include, first, analysis of the collected data on wind speed observed within the opening and in comparison to the roof mounted sensor and local weather station. Next, results are presented on the development of statistical regression-based models to estimate wind speed at the opening. Cross-validation is also used to evaluate model reliability.

Data Analysis

A summary of the data collected averaged to a 5-minute frequency, including the closest AWOS weather station data, is shown in Table 3. This includes average daily wind speed, and average and median wind speeds across the entire dataset.

Table 3. Average Wind Speed (m/s) for Dataset at a 5-minute Frequency

	S1 (1.22m)	S2 (2.44 m)	S3 (2.44 m)	S4 (3.66 m)	Average S (1,2,3,4)	S5 (13 m)	KLAN Weather Station (10 m)
Day 1 (n = 17)	0.91	0.70	0.85	0.77	0.81	5.60	6.29
Day 2 (n = 17)	0.70	0.46	0.53	0.57	0.57	3.31	3.33
Day 3 (n = 17)	0.64	0.48	0.54	0.61	0.57	3.49	6.54
Day 4 (n = 17)	0.56	0.56	0.42	0.55	0.52	3.45	4.60
Day 5 (n = 17)	1.02	1.01	0.69	0.60	0.83	6.32	7.02
Day 6 (n = 17)	0.51	0.37	0.34	0.42	0.41	1.58	1.94
Day 7 (n = 17)	1.61	1.40	1.35	0.99	1.34	9.53	5.42
Average (n = 7)	0.85	0.71	0.67	0.64	0.72	4.75	5.02
Median (n = 7)	0.70	0.56	0.54	0.60	0.58	3.49	5.42
Std Dev (n=7)	0.35	0.34	0.32	0.17	0.29	2.43	1.72

To better understand the distribution of wind speeds observed, Figure 2 presents boxplots of wind speed measurements recorded by sensors positioned within the opening (S1, S2, S3, S4, and S5) at five-minute intervals. Additionally, it includes data from the nearest AWOS weather station (KLAN) for comparison. The x-axis represents the sensor height (in meters) from the ground and the corresponding sensor number, while the y-axis indicates the wind speed (m/s) measured throughout the experiment.

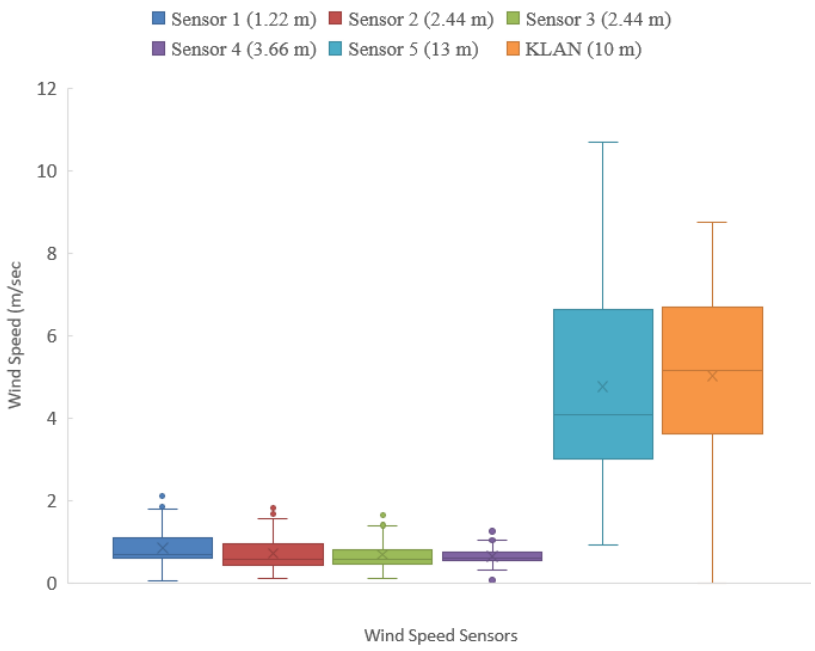

Figure 2: Boxplots of Wind Speeds by Sensors S1–S4 and AWOS KLAN (closest weather station) Data

From Table 3 the KLAN weather station, with an average wind speed of 5.02 m/s, closely aligns with the readings from Sensor 5 (roof-mounted), which recorded a slightly lower average of 4.75 m/s. Figure 2 further illustrates this comparison, showing that Sensor 5 had a first quartile (Q1) of 3.02 m/s and a third quartile (Q3) of 6.60 m/s. the KLAN weather station recorded a first quartile (Q1) of 3.60 m/s and a third quartile (Q3) of 6.43 m/s, indicating similar wind speed distributions with minor variations in dispersion. The Chi-square test resulted in a p-value of 0.2, which exceeds the 0.05 significance threshold, confirming that there is no statistically significant difference between the two distributions. This suggests that the wind speed measurements recorded at Sensor 5 and the KLAN weather station follow a similar distribution, supporting the use of regional weather data as a valid reference for local wind conditions in this case. The agreement between these sensors also suggests that wind speeds near the roof level are influenced by and similar to regional wind patterns. Additionally, this data shows that wind speeds were significantly higher at the roof level (Sensor 5) than at the opening, with an average speed of 4.75 m/s, which is nearly seven times greater than the opening-level mean of 0.72 m/s. Sensor 5 also exhibited significantly greater variability compared to the opening sensors (S1–S4).

Overall trends across the sensors at the opening suggest that the variability and magnitude of wind speed through the opening slightly decrease with an increase in height. Among the opening-level sensors, S1 (1.22 m) exhibited the highest mean speed of 0.85 m/s, whereas S4 (3.66 m) recorded the lowest at 0.64 m/s. These variations indicate that airflow distribution across the opening is not uniform but are much closer in magnitude than when comparing to the weather station data. The slightly elevated wind speeds at S1 suggest a greater contribution to infiltration at that location, whereas the lower speeds at S4 imply a slightly lower airflow, potentially resulting in lower infiltration rates in this area. The median wind speed values provide a more reliable measure of typical conditions, as they are less affected by extreme values. At S1 (1.22 m), the median (0.70 m/s) is lower than the mean (0.85 m/s), indicating skewness due to high wind speeds on certain days, such as 1.61 m/s on Day 7. Similarly, S5 (13 m) has a median of 3.49 m/s, significantly lower than its mean of 4.75 m/s, suggesting the influence of extreme values like 9.53 m/s on Day 7. In contrast, S4 (3.66 m) shows minimal difference between the mean (0.64 m/s) and median (0.60 m/s), indicating again a more balanced wind speed distribution at that height.

To better illustrate the relationship between sensor height and wind speed, wind speed profiles were created for each day of the experiment. Figure 3 illustrates the wind speed profiles for two different days (Day 1 and Day 4), focusing on sensors S1–S4 (excluding S5). Notably, the distribution of wind speeds is non-uniform, as higher sensors do not consistently record the strongest wind speeds, indicating variable airflow patterns at different heights.

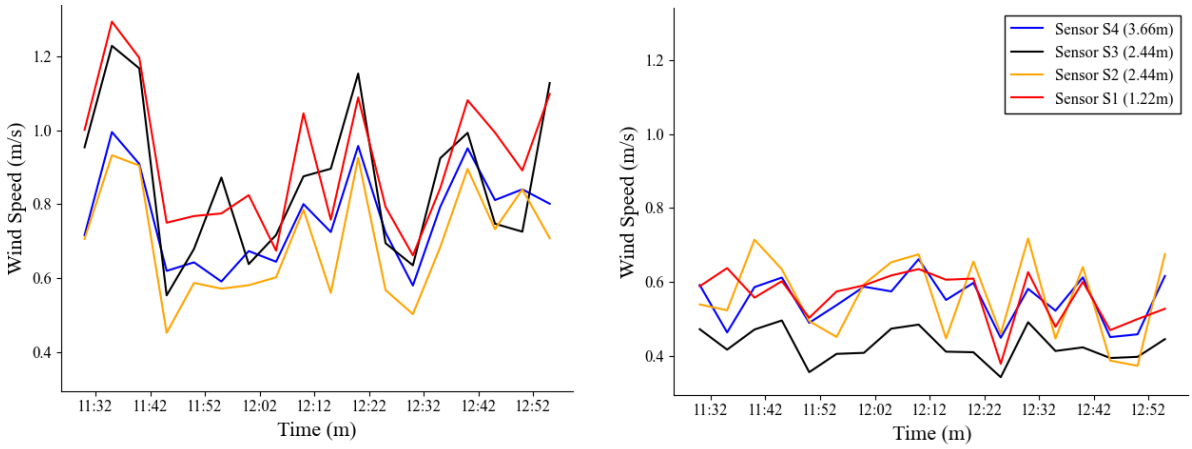

(a) **(b)**

Figure 3: Wind Speed Profiles Excluding S5 for (a) Day 1 and (b) Day 4

When considering all sensors, including Sensor 5 (5.2 m, roof level), Figure 4 shows how wind speeds at roof level are substantially higher (mean: 4.76 m/s) and much more variable (std dev: 2.58 m/s). This indicates that while airflow near the opening is relatively stable and influenced by ground-level conditions, wind exposure at higher elevations is significantly stronger and more variable, likely due to reduced obstructions and atmospheric effects.

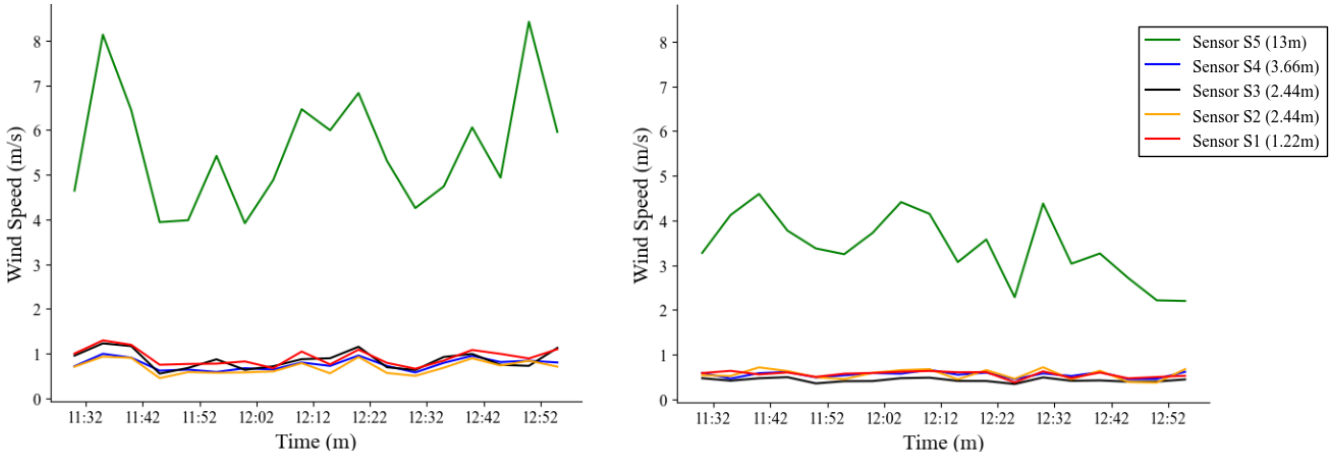

(a) **(b)**

Figure 4: Wind Speed Profiles Including S5 for Day 1 (a) and Day 4 (b)

To determine whether the observed differences were statistically significant, a t-test was conducted (Table 4). The t-test was used to compare the means of wind speeds at different sensor locations, helping to determine whether the differences observed were due to actual airflow dynamics rather than random variation. The results showed that the one-tailed p-value was less than 0.05 when comparing Sensor 1 with Sensors 2, 3, and 4, confirming that the wind speed recorded by Sensor 1 was significantly higher than that of Sensor 4. This statistical validation indicates that the differences observed were not due to random variation, but rather to localized factors influencing airflow at different heights.

Table 4. t-Test Results Comparing Means of Wind Speeds Captured by Sensor S1 vs. Sensors S2-S4

	S1 vs. S2	S1 vs. S3	S1 vs. S4
P values (one-tail)	1.42722E-54	5.41184E-82	1.6448E-107

Infiltration Rate Calculations

The infiltration rate (m^3/s) through the opening was next determined. In Approach 1, the infiltration rate was calculated using the average wind speed obtained from the nearest AWOS weather station (KLAN). Before being substituted in Equation 1 to calculate infiltration, the wind speed value was adjusted using Equation 2 to estimate the wind speed at the experimental location. In Approach 2, the infiltration rate was calculated by substituting the average wind speed measurements recorded by the sensors installed (S1,S2, S3, S4) at the opening directly in Equation 1. The results are shown in Table 5.

Table 5. Results of Infiltration Rate (m^3/s) Analysis

	Wind Speed (m/s)	Adjusted Wind Speed (m/s)	Infiltration (m^3/s)	Percentage Difference
Approach 1 – Using KLAN weather station data and Equation 2	5.02	1.74	16.41*	-
Approach 2 - Using (S1, S2, S3, S4) averaged data	0.68	NA	6.42	60.90% (Reduction)

***The infiltration rate was calculated using the matching adjusted wind speed.

When using Approach 1, the adjusted wind speed at the experimental location was 1.74 m/s, resulting in an estimated infiltration rate of 16.41 m^3/s. In contrast, when using the on-site sensor data (Approach 2), the recorded average wind speed across the sensors within the large opening (S1,S2,S3,S4) was significantly lower at 0.68 m/s, leading to a lower infiltration rate of 6.42 m^3/s estimation. This difference corresponds to a 60.9% reduction in wind speed and decrease in the estimated infiltration rate (m^3/s) when using on-site sensor data instead of Equation 2.

Data-Driven Model Development and Validation

To establish a data driven model to relate weather station height wind data to air speeds occurring at large openings, data-driven statistical modeling techniques were next employed to develop predictive relationships between measured wind speeds at the weather station height and wind speeds at the openings. Two different modeling approaches were implemented.

In the first approach, the regression model included sensor height (x_1) and the average wind speed captured by Sensor 5 installed on the roof (x_2) as predictor variables. This approach was intended to evaluate whether height contributed to explaining variations in infiltration rates. In the second approach, height was excluded as a variable, and the model was developed using only the wind speed captured by Sensor 5 as the predictor variable. Table 6 shows the regression model format, resulting values for each variable, and the resulting coefficient of variation (R^2).

Table 6. Summary of Regression Models (Approach 1 & 2) for Estimating Wind Speed Through the Opening

No	Type	Model Equation	Variables	R^2
Model 1 (Approach 1, w/ sensor height)	Linear	$y = a_1x_1 + a_2x_2 + b$	a_1= -0.09 (p-value= 7.19e-15) a_2= 0.11 (p-value= 2.47e-84) b = 0.44 (p-value= 1.80e-32)	0.68
Model 2 (Approach 1, w/ sensor height)	Linear Poly-nomial	$y = a_1x_1 + a_2x_2 + a_3{x_1}^2 + + a_4{x_2}^2 + a_5x_1x_2 + b$	a_1= -0.06 (p-value= 3.78-01) a_2= 0.10 (p-value= 3.91-08) a_3= 0.05 (p-value= 7.12e-02) a_4= -0.03 (p-value= 2.87e-15) a_5= 0.01 (p-value= 4.74e-07) b = 0.38 (p-value= 2.81e-05)	0.75
Model 3 (Approach 1, w/ sensor height)	Non-linear	$y = a_1 e^{a2 .x1} + a_3 x_2 + b$	a_1= -587 (p-value= 0.99) a_2=0.0001 (p-value= 0.99) a_3= 0.11 (p-value= 0) b = 587 (p-value= 0.99)	0.68
Model 1 (Approach 2, no height)	Linear	$y = a_1x_1 + b$	a_1= 0.24 (p-value= 1.92e-40) b = 0.10 (p-value= 8.26e-15)	0.76

To assess the reliability and generalizability of the regression models developed in Approach 1 and 2, two validation techniques were employed: subset validation using a portion of the training dataset and K-fold cross-validation. For subset validation, a subset of the dataset, specifically two random days of data from the original dataset (28%), were used to test how well the models performed on a portion of the data that was included in model development.

The R-squared (R^2) values obtained for this validation for Model 1, Model 2 and Model 3 for Approach 1 are 0.82. 0.89 and 0.82 respectively, and 0.76 for Model 1 of Approach 2. These results suggest that the models performed better when tested on this subset than on the overall dataset, particularly the polynomial model, which showed the strongest predictive capability. For the second validation approach, 5-fold cross-validation was performed using the entire dataset for both Approach 1 and 2. This method mitigates overfitting by dividing the data into five subsets, training the model on four subsets, and validating it on the remaining subset in an iterative process. The average R-squared values across the five folds For Approach 1 and 2 are presented in Table 7.

Table 7. Average R-squared Values Across Five Folds For Regression Models

No	R^2 K-Fold Average	R^2 Fold 1	R^2 Fold 2	R^2 Fold 3	R^2 Fold 4	R^2 Fold 5
Model 1 (Approach 1)	0.67	0.60	0.69	0.74	0.69	0.65
Model 2 (Approach 1)	0.75	0.83	0.74	0.71	0.77	0.70
Model 3 (Approach 1)	0.68	0.78	0.65	0.68	0.68	0.62
Model 1 (Approach 2)	0.76	0.72	0.62	0.81	0.81	0.84

For Approach 1, the cross-validation results suggest that the polynomial model offers the best predictive capability while the linear and non-linear models perform similarly but slightly less quality prediction. This suggests that the polynomial model better captures non-linear relationships in the data. However, the moderate R^2 values suggest that the models may benefit from addition predictive variables that could increase further. In addition, as the cross-validation R^2 value remained the same (0.76) indicates that the model is not overfitting and is similarly performing across different data partitions. For Approach 2, the model yielded an average R^2 value of 0.76, confirming that the model generalizes well across different subsets of the dataset.

Modeled vs. Predicted Data

To further evaluate the performance of the regression model developed in Approach 2, the model was used to predict wind speed through the opening. The predicted wind speed values were then compared against the actual measured wind speeds (averaged values of sensors S1, S2, S3,S4). The results are presented in Figure 5 below, which illustrates the relationship between actual and predicted values. A strong alignment between the two sets of values indicates high model accuracy, whereas significant deviations would suggest potential sources of error or missing predictive factors. Given that the model achieved an R^2 value of 0.76, the visualization provides further validation of estimating wind speed through the opening based on on-site sensor data.

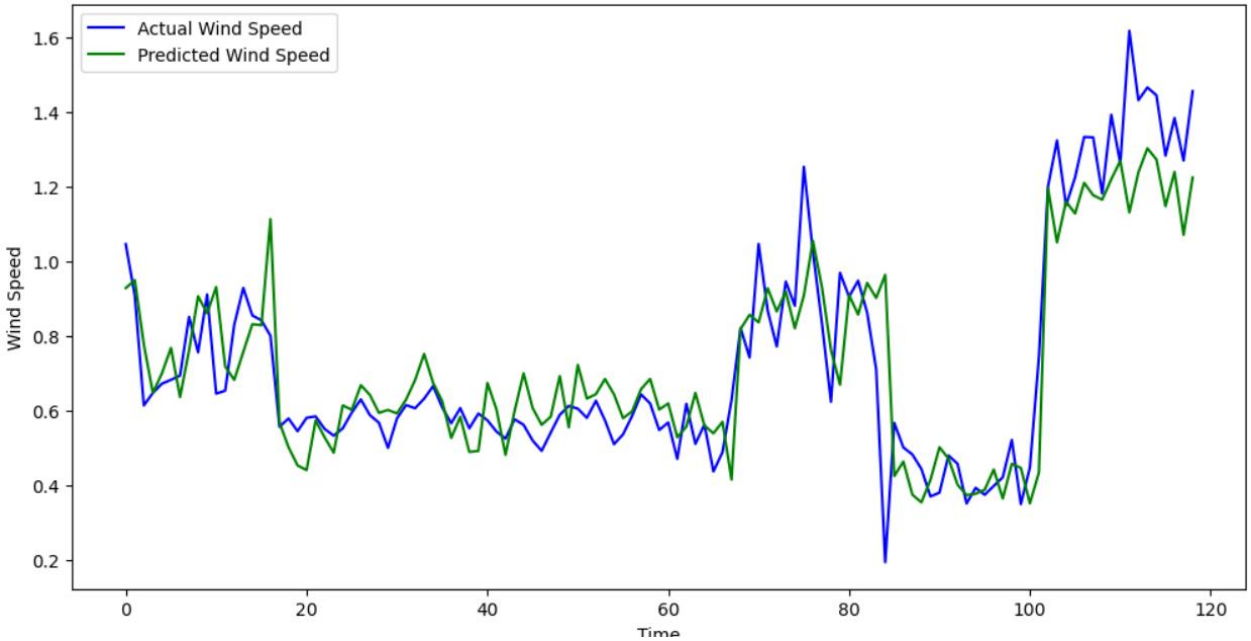

Figure 5: Comparison of Actual vs. Predicted Average Wind Speeds of Sensors S1, S2, S3, S4 for Approach 2 Regression Model

CONCLUSIONS

This study investigated air infiltration through large vertical openings in buildings using wind speed data collected from on-site sensors in a single-zone industrial building, with the goal of developing a new empirical-based estimation method for predicting wind speed and thus infiltration through these large openings using weather data. Results suggest that:

- Wind speeds varied across the opening, with higher sensors not consistently recording the higher windspeeds, indicating variable airflow patterns at different heights.
- Infiltration rates derived from on-site sensor data were 60.90% lower compared to estimates obtained using EnergyPlus wind-drive infiltration model "Effective Leakage Area Model" .
- Four regression models were developed to estimate wind speed at large openings based on weather data for use in infiltration rate calculations. The best-performing model, (Model 1 in Approach 2 - Linear), achieved the highest average R^2 value of 0.76.

There are some limitations of this study. Data was collected over a multi-day period in one climate zone and a single size opening. This may limit the applicability of the findings of this study as there are a broad range of climate zones and large opening sizes that can occur in buildings. Future research would benefit from incorporating long-term data covering multiple climates or longer periods to capture wind variations and assess the long-term stability of the findings. Future research would also benefit from assessing impacts on findings using different opening sizes to improve the generalizability of the models. Additional variables impacting wind speed occurring at large openings could also be studied, such as direction of the wind, orientation of openings, and environmental variables such as temperature, humidity, and pressure differentials.

The results of this study have important implications for energy efficiency strategies, building design, and HVAC optimization. From an energy efficiency perspective, the lower infiltration rate estimated using on-site sensor data indicates that heat losses due to wind-driven infiltration may be significantly lower than initially estimated based on the use of Equation 2 from EnergyPlus wind-drive infiltration model "Effective Leakage Area Model". This has direct implications for energy savings calculations in industrial facilities, as heating and cooling loads associated with infiltration maybe overestimated. By utilizing the proposed empirical relationships between

weather station wind speed and those measured at large openings, the results of this research can help facilities to achieve a more accurate assessment of their energy losses, leading to better-informed energy conservation strategies and potentially reducing unnecessary investments in infiltration mitigation measures.

BIBLIOGRAPHY

Allard, F., & Utsumi, Y. (1992). Airflow through large openings. Energy and Buildings, 18(2), 133–145. https://doi.org/10.1016/0378-7788(92)90042-F

Andrews, A., & Jain, R. K. (2023). Evaluating building decarbonization potential in U.S. cities under emissions-based building performance standards and load flexibility requirements. Journal of Building Engineering, 76, 107375. https://doi.org/10.1016/j.jobe.2023.107375

ASHRAE. (2020). ANSI/ASHRAE Standard 119-2020: Air leakage performance for detached single-family residential buildings. American Society of Heating, Refrigerating and Air-Conditioning Engineers.

ASHRAE. (2021). ASHRAE climate data. American Society of Heating, Refrigerating and Air-Conditioning Engineers. Retrieved March 01, 2025, from https://ashrae-meteo.info/v2.0/

ASHRAE. (2021). ASHRAE handbook: Fundamentals. American Society of Heating, Refrigerating and Air-Conditioning Engineers.

ASTM. (2021a). Standard test method for determining air leakage rate by fan pressurization (ASTM E779-19). ASTM International. https://www.astm.org/e0779-19.html

ASTM. (2021b). Standard test method for determining air change in a single zone by means of a tracer gas dilution (ASTM E741-11(2017)). ASTM International. https://www.astm.org/e0741-11r17.html

Banti, N. (2024). Existing industrial buildings – A review on multidisciplinary research trends and retrofit solutions. Journal of Building Engineering, 84, 108615. https://doi.org/10.1016/j.jobe.2024.108615

Basse, A., Callies, D., Grötzner, A., & Pauscher, L. (2021). Seasonal effects in the long-term correction of short-term wind measurements using reanalysis data. Wind Energy Science, 6, 235–245. https://doi.org/10.5194/wes-2020-134

Bawaneh, K., Overcash, M., & Twomey, J. (2017). Industrial facilities nonprocess energy. Critical Reviews in Environmental Science and Technology, 47(23), 2259–2274. https://doi.org/10.1080/10643389.2013.782168

Brinks, P., Kornadt, O., & Oly, R. (2015). Air infiltration assessment for industrial buildings. Energy and Buildings, 86, 663–676. https://doi.org/10.1016/j.enbuild.2014.10.040

Brinks, P., Kornadt, O., & Oly, R. (2016). Development of concepts for cost-optimal nearly zero-energy buildings for the industrial steel building sector. Applied Energy, 173, 343–354. https://doi.org/10.1016/j.apenergy.2016.04.007

Brown, R., Borgeson, S., Koomey, J., & Biermayer, P. (2008). U.S. building-sector energy

efficiency potential. Environmental Energy Technologies Division, Ernest Orlando Lawrence Berkeley National Laboratory, University of California. https://[Insert URL if available]

Campbell Scientific, Inc. (2023). CR1000X measurement and control datalogger: Product manual (Rev. 11/2023). Campbell Scientific, Inc. https://s.campbellsci.com/documents/au/manuals/cr1000x-product-manual.pdf

Choi, K., Park, S., Joe, J., Kim, S.-I., Jo, J.-H., Kim, E.-J., & Cho, Y.-H. (2023). Review of infiltration and airflow models in building energy simulations for providing guidelines to building energy modelers. Renewable and Sustainable Energy Reviews, 181, 113327. https://doi.org/10.1016/j.rser.2023.113327

Deng, X., & Tan, Z. (2019). Numerical analysis of local thermal comfort in a plan office under natural ventilation. Indoor and Built Environment. https://doi.org/10.1177/1420326X19866497

Dong, H., Srivastava, A., Cetin, K., & Mitra, D. (2024). Socioeconomic factors influencing residential occupancy trends during and post COVID pandemic. Science and Technology for the Built Environment, 30(9), 1070–1084. https://doi.org/10.1080/23744731.2024.2386881

Economidou, M., Todeschi, V., Bertoldi, P., D'Agostino, D., Zangheri, P., & Castellazzi, L. (2020). Review of 50 years of EU energy efficiency policies for buildings. Energy and Buildings, 225, 110322. https://doi.org/10.1016/j.enbuild.2020.110322

Edelson, J., & Cheslak, K. (2021). The technical basis of building performance standards. New Buildings Institute.

Emmerich, S., & Persily, A. (2014). Analysis of U.S. commercial building envelope air leakage database to support sustainable building design. International Journal of Ventilation, 12(4), 331–344.

Federal Aviation Administration. (2017). Automated weather observing systems (AWOS) for non-federal applications (Advisory Circular No. 150/5220-16E). U.S. Department of Transportation. https://www.faa.gov/documentLibrary/media/Advisory_Circular/150-5220-16E.pdf

González-Torres, M., Pérez-Lombard, L., Coronel, J. F., Maestre, I. R., & Yan, D. (2022). A review on buildings energy information: Trends, end-uses, fuels, and drivers. Energy Reports, 8, 626–637. https://doi.org/10.1016/j.egyr.2021.11.280

Gourlis, G., & Kovacic, I. (2016). A study on building performance analysis for energy retrofit of existing industrial facilities. Applied Energy, 184, 1389–1399. https://doi.org/10.1016/j.apenergy.2016.03.104

Gowri, K., Winiarski, D., & Jarnagin, R. (2009). Infiltration modeling guidelines for commercial building energy analysis. U.S. Department of Energy. https://www.pnnl.gov/main/publications/external/technical_reports/PNNL-18898.pdf

Hayati, A. (2017). Natural ventilation and air infiltration in large single-zone buildings: Measurements and modelling with reference to historical churches [Doctoral dissertation, University of Gävle]. DiVA Portal. https://www.diva-portal.org/smash/get/diva2:1117979/FULLTEXT01.pdf

Hayati, A., Mattsson, M., & Sandberg, M. (2018). A wind tunnel study of wind-driven airing through open doors. International Journal of Ventilation, 18(2), 113–135. https://doi.org/10.1080/14733315.2018.1435027

International Code Council. (2015). 2015 International building code (IBC). International Code Council. https://codes.iccsafe.org

International Energy Agency. (2019). Multiple benefits of energy efficiency 2019. IEA. https://www.iea.org/reports/multiple-benefits-of-energy-efficiency-2019

International Energy Agency. (2025). Buildings. International Energy Agency. Retrieved March 01,2025, from https://www.iea.org/energy-system/buildings

Jokisalo, J., Kurnitski, J., Korpi, M., Kalamees, T., & Vinha, J. (2009). Building leakage, infiltration, and energy performance analyses for Finnish detached houses. Building and Environment, 44(2), 377–387. https://doi.org/10.1016/j.buildenv.2008.03.014

Jones, B., Das, P., Chalabi, Z., Davies, M., Hamilton, I., Lowe, R., Mavrogianni, A., Robinson, D., & Taylor, J. (2015). Assessing uncertainty in housing stock infiltration rates and associated heat loss: English and UK case studies. Building and Environment, 92, 644–656. https://doi.org/10.1016/j.buildenv.2015.05.033

Kempton, L., Daly, D., Kokogiannakis, G., & Dewsbury, M. (2022). A rapid review of the impact of increasing airtightness on indoor air quality. Journal of Building Engineering, 57, 104798. https://doi.org/10.1016/j.jobe.2022.104798

Kirimtat, A., & Krejcar, O. (2018). Air leakage. Energy and Buildings. https://doi.org/10.1016/j.enbuild.2018.01.033

Kosonen, R., Jokisalo, J., Ranta-aho, I., & Koikkalainen, E.-P. (2017). Methods to reduce stack effect and improve energy efficiency in a Nordic high-rise residential building. Procedia Engineering, 205, 2311–2317. https://doi.org/10.1016/j.proeng.2017.10.118

Lackner, M. A., Rogers, A. L., & Manwell, J. F. (2008). Uncertainty analysis in MCP-based wind resource assessment and energy production estimation. Journal of Solar Energy Engineering, 130(3), 031006. https://doi.org/10.1115/1.2931499

Liu, X., Liu, X., & Zhang, T. (2020). Theoretical model of buoyancy-driven air infiltration during heating/cooling seasons in large space buildings. Building and Environment, 173, 106735. https://doi.org/10.1016/j.buildenv.2020.106735

Liu, Y., Mao, W., & Diaz-Elsayed, N. (2022). An investigation of the indoor environment and its influence on manufacturing applications via computational fluid dynamics simulation. Building and Environment, 219, 109161. https://doi.org/10.1016/j.buildenv.2022.109161

Makawi, M. A., Budaiwi, I. M., & Abdou, A. A. (2023). Characterization of envelope air leakage behavior for centrally air-conditioned single-family detached houses. Buildings, 13(3), Article 660. https://doi.org/10.3390/buildings13030660

Mannan, M., & Al-Ghamdi, S. G. (2021). Indoor air quality in buildings: A comprehensive review on the factors influencing air pollution in residential and commercial structures. International Journal of Environmental Research and Public Health, 18(6), Article 3276. https://doi.org/10.3390/ijerph18063276

METER Group. (n.d.). ATMOS 22 ultrasonic anemometer: Technical specifications. METER Group. Retrieved [Month Day, Year], from https://metergroup.com/products/atmos-22/atmos-22-tech-specs/

NAIOP. (2024). Commercial real estate terms and definitions. NAIOP. https://www.naiop.org/education-and-career/industry-terms-and-definitions/
National Association of Manufacturers. (2025). Manufacturing in the United States. National Association of Manufacturers. https://nam.org/mfgdata/

National Weather Service. (2025). Current conditions for Capital Region International Airport (KLAN). U.S. Department of Commerce. Retrieved [Month Day, Year], from https://forecast.weather.gov/MapClick.php?x=247&y=189&site=grr&zmx=&zmy=&map_x=247&map_y=189

Ng, L. C., Zimmerman, S., Good, J., Toll, B., Emmerich, S. J., & Persily, A. K. (2019). Estimating real-time infiltration for use in residential ventilation control. Indoor and Built Environment. Advance online publication. https://doi.org/10.1177/1420326X19870229

Persily, A., Ng, L., Dols, W. S., & Emmerich, S. J. (2019). Techniques to estimate commercial building infiltration rates. Proceedings of the 40th AIVC - 8th TightVent & 6th venticool Conference.

Porsani, G. B., Fernández-Vigil Iglesias, M., Echeverría Trueba, J. B., & Fernández Bandera, C. (2024). Infiltration models in EnergyPlus: Empirical assessment for a case study in a seven-story building. Buildings, 14(2), Article 421. https://doi.org/10.3390/buildings14020421

Sakiyama, N. R. M., Carlo, J. C., Sakiyama, F. I. H., Abdessemed, N., Frick, J., & Garrecht, H. (2024). Impact of wind pressure coefficients on the natural ventilation effectiveness of buildings through simulations. Buildings, 14(9), Article 2803. https://doi.org/10.3390/buildings14092803

Sherman, M. H., & Grimsrud, D. T. (1980). Air infiltration measurement techniques. Lawrence Berkeley National Laboratory. https://doi.org/10.2172/5292881

Shoemaker, S. (2023, September 14). NREL researchers reveal how buildings across United States do—and could—use energy: New data set reveals how improvements to U.S. buildings could reduce carbon emissions and increase occupant comfort. National Renewable Energy Laboratory.

Sun, H., & Yang, Q. (2014). Influence of infiltration on energy consumption of a winery building. Frontiers in Energy, 8(1), 110–118. https://doi.org/10.1007/s11708-013-0293-3

Tanasić, N., Jankes, G., & Skistad, H. (2011). CFD analysis and airflow measurements to approach large industrial halls energy efficiency: A case study of a cardboard mill hall. Energy and Buildings, 43(6), 1200–1206. https://doi.org/10.1016/j.enbuild.2010.12.034

U.S. Bureau of Labor Statistics. (2022, January 5). Injuries, illnesses, and fatalities: Snapshots. U.S. Department of Labor. Retrieved March 01, 2025, from https://www.bls.gov/iif/publications/snapshots.htm

U.S. Bureau of Labor Statistics. (2025). Industry at a glance. U.S. Department of Labor. Retrieved March 01, 2025, from https://www.bls.gov/iag/

U.S. Department of Energy. (2015). Quadrennial technology review: An assessment of energy technologies and research opportunities – Chapter 5: Increasing efficiency of building systems and technologies. U.S. Department of Energy. https://www.energy.gov

U.S. Department of Energy. (2022). EnergyPlus™ Version 22.1.0: Engineering reference manual. U.S. Department of Energy. https://energyplus.net/documentation

U.S. Department of Transportation. (2004). Truck size and weight regulations (23 C.F.R. § 658). U.S. Government Publishing Office. https://www.ecfr.gov

U.S. Energy Information Administration. (2023, October 11). [Title of the press release]. U.S. Energy Information Administration. https://www.eia.gov/pressroom/releases/press542.php#:~:text=The%20U.S.%20Energy%20Information%20Administration,Energy%20Outlook%202023%20(IEO2023).

U.S. Energy Information Administration. (2018). Manufacturing energy consumption survey (MECS), 2018. U.S. Department of Energy. https://www.eia.gov/consumption/manufacturing/

Wang, Y., Cao, Y., & Meng, X. (2019). Energy efficiency of industrial buildings. Indoor and Built Environment, 28(3), 298–313. https://doi.org/10.1177/1420326X19826192

Wilberforce, T., Olabi, A. G., Sayed, E. T., Elsaid, K., Maghrabie, H. M., & Abdelkareem, M. A. (2023). A review on zero energy buildings – Pros and cons. Energy and Built Environment, 4(1), 25–38. https://doi.org/10.1016/j.enbenv.2021.06.002

Younes, C., Abi Shdid, C., & Bitsuamlak, G. (2012). Air infiltration through building envelopes: A review. Journal of Building Physics, 35(3), 267–302. https://doi.org/10.1177/1744259111423085